applied nano

MDPI

Article

Inkjet-Printed Conductive Patterns on Electrospun Substrates for the Modular Fabrication of Nonplanar Circuits

Fabricio N. Molinari [1], Emanuel Bilbao [2] and Leandro N. Monsalve [3,4,5,*]

[1] Department of Chemical, Biological, Pharmaceutical and Environmental Sciences, University of Messina, 98158 Messina, Italy; fmolinari@unime.it
[2] Instituto Nacional de Tecnología Industrial (INTI) Nanomateriales Funcionales, San Martín B1650WAB, Buenos Aires, Argentina; ebilbao@inti.gob.ar
[3] Instituto Nacional de Tecnología Industrial (INTI) Textiles, San Martín B1650WAB, Buenos Aires, Argentina
[4] Consejo Nacional de Investigaciones Científicas y Técnicas (CONICET-INTI), San Martín B1650WAB, Buenos Aires, Argentina
[5] Instituto de Calidad Industrial (INTI-UNSAM), San Martín B1650WAB, Buenos Aires, Argentina
* Correspondence: monsalve@inti.gob.ar; Tel.: +54-11-4724-6200 (ext. 6714)

Abstract: Placing printed conductive patterns onto nonplanar substrates is a challenging task. In this work, we tested a simple method for depositing inkjet-printed conductive patterns onto 3D-printed pieces with cavities and sharp edges. First, a silver nanoparticle ink was used to print conductive patterns onto a flexible and porous substrate made of electrospun polycaprolactone (PCL). Then, the printed patterns were transferred to 3D-printed pieces made of polylactic acid (PLA) by temperature-promoted adhesion. Finally, the printed patterns were cured to render them conductive. The influence of the number of printed layers on their electrical and mechanical properties was evaluated. The printed patterns were also transferred to flexible substrates, such as thermoplastic polyurethane (TPU) and polyethylene terephthalate (PET) sheets, achieving conductivity after curing. Moreover, the printed patterns were effective for modular interconnection among successive transferred patterns, since it was possible to achieve electrical contact between them during the transfer process.

Keywords: printed electronics; electrospinning; 3D printing; printed transfers

Academic Editor: Johann Michael Köhler

Received: 25 April 2025
Revised: 10 June 2025
Accepted: 11 June 2025
Published: 18 June 2025

Citation: Molinari, F.N.; Bilbao, E.; Monsalve, L.N. Inkjet-Printed Conductive Patterns on Electrospun Substrates for the Modular Fabrication of Nonplanar Circuits. *Appl. Nano* **2025**, *6*, 10. https://doi.org/10.3390/applnano6020010

1. Introduction

The fabrication of printed devices and circuits onto nonplanar substrates is a challenge yet to overcome in order to trespass the prototype scale and jump to more reliable and reproducible industrial production. Although effective for prototype fabrication, current fabrication approaches are slow and complex or deal with compatibility and mechanical strain issues between substrates and printing materials when subjected to deformation. Potential massive applications to nonplanar circuits are broad, including automotive, aerospace, wearables and skin electronics, among many others.

Several approaches can be used for the fabrication of devices and circuits on nonplanar substrates. Conductive tracks can be fabricated directly onto nonplanar surfaces by the deposition of conductive materials using electrodeposition [1], plasma jet [2], vapor deposition, extrusion [3], inkjet or aerosol-jet printing [4]. For example, quantum dot LEDs could be already printed directly onto nonplanar surfaces by carefully selecting different combinations of materials [5]. Both approaches suffer from some drawbacks: a shadow mask or complex lithographic methods have to be used in order to print lines on the surface of a nonplanar piece, whereas aerosol-jet and inkjet printing are slow on

nonplanar substrates, requiring very precise and complex numeric control (x, y, z, φ and θ) for printing onto 3D substrates. Three-dimensional printing is also being used for the fabrication of nonplanar circuits. In this case, the piece and the embedded circuit can be fabricated at the same time, which thus seems to be the best approach in terms of degrees of freedom regarding design. Three-dimensional and inkjet printing have been used for the fabrication of batteries and interconnections by tailoring processes and nanocomposites with different functional materials [6–9]. However, fine line resolution is not achievable, and the performance of conductive materials for 3D printing must be further optimized. For instance, Izumi et al. developed a method called soft blanket gravure, which consist of transferring a gravure pattern to a soft blanket, which in turn transfers it to the printing substrate. The highly deformable blanket allows transfer processes on nonplanar substrates. However, as the fidelity of the printed pattern depends on the printing pressure and the viscoelastic characteristics of the ink, this method must be carefully tuned for each ink and shape of the printing substrate [10].

On the other hand, circuits can be also printed onto planar substrates prior to molding them into a particular shape. For instance, Bakr et al. studied the integrity and functionality of copper conductive tracks deposited on a flexible substrate after embedding it in a 3D plastic piece by injection molding using different plastics [11]. Another example of this approach is the work from Sundaram et al., in which self-shaping substrates were 3D-printed, then electrically conductive patterns were inkjet-printed, and finally the substrate self-folded once it was peeled off from the printing bed. This approach requires careful design of the 3D-printed substrate, and the achievable shapes are limited [12]. Special care must be taken in these cases to prevent cracking or delamination of the printed layers, as it becomes very complex to match adhesion, mechanical and thermal properties between the substrate and the printed layers while maintaining functionality. Another variation of this approach consists of printing the circuit onto a planar, flexible and adhesive substrate which is stuck to the surface of a 3D or flexible object afterwards. This approach has been already used for in-mold electronics, soft robots [13] and skin electronics. For instance, Miyamoto et al. fabricated an electrospun mat made of polyvinyl alcohol with deposited conductive tracks made of gold by vacuum deposition using a shadow mask [14]. This mat could be transferred to various substrates by dissolving the PVA with a water spray. Interestingly, a hydroprinting method for transferring conductive patterns from PVA films to 3D structures has been proposed.

Electrospinning is a very versatile technique for the fabrication of micro- and nanoporous membranes for a wide variety of applications. It can be used for the fabrication of nonwoven mats from a variety of materials, including thermoplastic polymers. Our group has been working on the fabrication of conductive electrospun mats based on polycaprolactone (PCL) for the fabrication of electronic devices [15,16]. PCL is a synthetic biodegradable polyester that has a low glass transition temperature (−60 °C), low melting point (60 °C) and excellent flexibility. Moreover, PCL has low interfacial tension [17], and it has been demonstrated previously that PCL can be adhered to polylactic acid (PLA) by deposition of molten PCL onto 3D-printed PLA pieces by fused deposition modeling (FDM) [18].

Electrospun mats can be either planar or 3D-shaped, depending on the characteristics of the collector used. Moreover, electrospun fibers can be deposited as a surface layer onto 3D-printed objects. For instance, a recent paper from Saniei et al. reported the surface modification of 3D-printed screws made of polylactide (PLA) with electrospun fibers in order to improve their bioactivity [19].

Although it has been reported that conductive materials can be deposited onto electrospun mats and electrospun mats can be used as a surface layer for 3D-printed objects in order to improve their functionality, inkjet printing of conductive materials onto electrospun mats and their use for transferring to 3D-printed objects has not been previously studied. In this work, a method for the fabrication of conductive tracks onto electrospun mats made of polycaprolactone (PCL) by inkjet printing is presented. These mats were transferred to different plastic planar and nonplanar surfaces by melting the PCL, leaving the conductive track adhered and functional.

2. Materials and Methods

2.1. General Remarks

PCL (Mw 80000, Sigma-Aldrich, CABA, Argentina) was used for electrospinning. DMF (99.8%, Biopack, Buenos Aires, Argentina) and chloroform (99.8%, Ciccarelli, Rosario, Argentina) were reagent-grade and used straight from the bottle. White PLA filament for 3D printing of 1.75 mm diameter was purchased from Grilon (Buenos Aires, Argentina) and used for 3D printing. Baking paper (50 g/m^2), kraft paper (75 g/m^2) and sulfite paper (80 g/m^2) were purchased from a local seller. Silver nanoparticle ink DGP 40LT-15C from Advanced Nano Products was used for inkjet printing.

2.2. Preparation of Polymer Solutions

A total of 1.2 g of PCL was dissolved in 10 mL of a mixture of chloroform–DMF at 80:20, respectively, under magnetic stirring for 4 h. The solution has demonstrated stability for at least two weeks after preparation.

2.3. Fabrication of Electrospun Mats

A Y-flow electrospinner 2.2.D-500 (Y-flow SD, Málaga, Spain) was used for electrospinning. Distance to the collector was optimized in order to obtain regular and dry fibers. Distance was determined as 26 cm as the optimum distance between the needle and the collector. The flow rate of the solution was 1 $mL.h^{-1}$. A rotary drum collector was employed to produce mats of aligned fibers. The set up included two high voltage sources: the needle source was settled between +6 and +12 kV and the collector between −15 and −17 kV. The fibers have been collected onto different substrates (sulfite paper, baking paper and kraft paper) to determine the better substrate to allow the printing process and transfer process.

2.4. Inkjet Printing Process

Silver ink patterns were printed with a Dimatix Materials Printer 2850 (Fujifilm, NY, USA). The printer plate was set to 40 °C for all printed patterns. For every fiber mat, 9 electrodes were printed, with a fixed length of 15 mm, and different combinations of the number of layers (1 to 6 layers) and width of the electrodes (250, 500 and 1000 μm), using a resolution of 726 dpi. For assessing the rub resistance, electrodes were printed, having length and width dimensions of 20 mm and 1 mm, respectively. These electrodes had a number of layers ranging from 2 to 6 and a resolution of 726 dpi. The geometry of the printed tracks is shown in Figure 1.

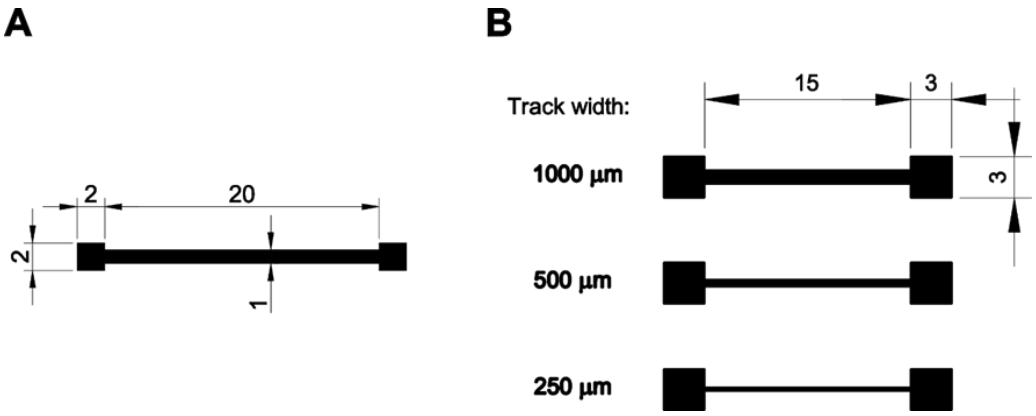

Figure 1. Design of printed tracks for rub resistance (**A**) and electrical and dimensional characterization (**B**).

2.5. 3D Printing and Transfer Process

PLA orthohedra were 3D-printed using a Makerparts 1 3D printer (3D insumos, Caseros, Argentina). The bed temperature was set at 60 °C, and the extruder temperature was set at 210 °C. A nozzle of 0.4 mm was used, and the layer height was set at 0.2 mm. The printing speed was set at 60 mm/s. No post-treatment was performed on 3D-printed substrates. Fibers with printed patterns were transferred by contacting the printed face of the mat to different substrates such as PET film, TPU film and planar and nonplanar PLA 3D-printed pieces. The substrates were previously heated at 80 °C, and after the transfer process, they were cured at 145 °C for 45 min in an oven.

2.6. Characterization

Scanning electron microscopy experiments were performed in a FEI Quanta 250 FEG (FEI, Hillsboro, FL, USA). The fiber morphology and printed layer morphology before and after each step of the transfer process were analyzed by SEM. Electrical characterization was performed using a Fluke 75III calibrated multimeter. Rub resistance was measured by adapting a standard ISO 105-A01:2010-01 [20] apparatus using a crockmeter James Heal 255A (VA, USA) without additional weight. Profiles were obtained using a Bruker Dektak XT. Adherence tests were performed by taping Scotch-brand adhesive tape (3M, Argentina) with a pressure of 10 N cm^{-2} on the sensors, removing the tape and scanning the material removed by the tape with a desktop scanner.

3. Results

3.1. Optimization of Printing Substrate

Since the PCL mat is porous, a sheet underneath must be used for printing in order to prevent the ink from leaching. The surface characteristics of the material underneath the paper, compared to PCL fibers, will influence the printability and functionality of the printed layers. A silver nanoparticle ink was used for printing 15 mm long tracks with different widths (0.25, 0.5 and 1 mm) in order to evaluate the printability and functionality of the printed pattern. Four materials were used underneath the PCL electrospun mat: kraft paper, sulfite paper and baking paper (Figure 2).

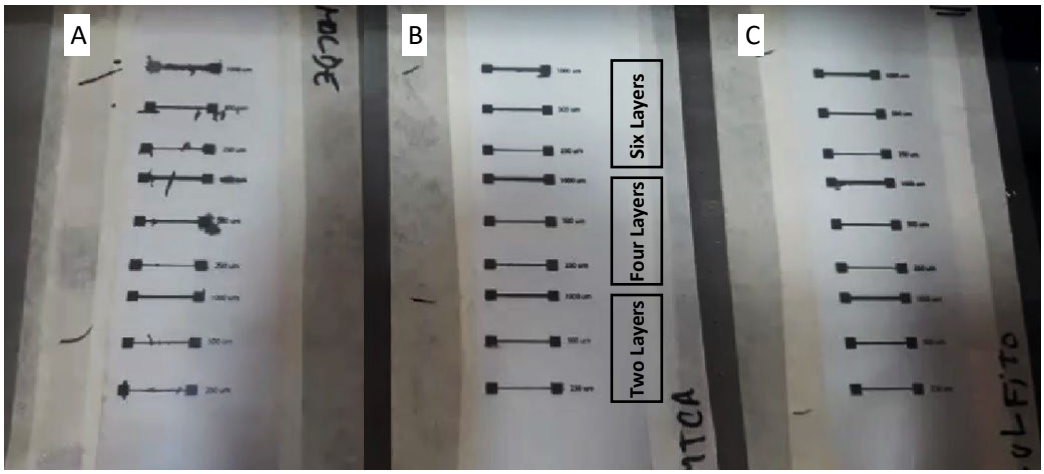

Figure 2. Tracks with incremental printed layers on PCL onto kraft paper (**A**), baking paper (**B**) and sulfite paper (**C**) after the printing process.

As can be seen in Figure 2, PCL onto kraft paper yielded very poor results in terms of printability, leading to noticeable ink spreading. On the other hand, the other substrates led to reasonably well-shaped patterns.

The surface energy of the substrates seems to play an important role regarding the fidelity of the printed patterns. Kraft paper has the highest surface energy and tends to absorb the ink from the PCL mat, whereas the other substrates have lower surface energy and thus help to keep the ink in the PCL mat. As the PCL layer readily absorbs the ink, the baking paper serves as a layer of low surface energy that repels the ink, helping to keep it inside the PCL layer. Baking paper also provides mechanical support for handling the printed patterns and can be easily peeled off from the PCL layer during the transfer process. The optimal transfer temperature that ensures the adhesion of PCL to PLA was found to be 80 °C. The optimization steps are detailed in the Supplementary Materials.

Noticeable differences could be observed in the fidelity of the printed patterns between the substrates, revealing the influence of the characteristics of the printing substrate on the printing process. Differences in the diffusion of the ink trough along and across the fiber length were also noticeable and probably associated with interactions between ink and the PCL mat. The occurrence of ink absorbed by the sulfite paper and kraft paper revealed the presence of a diffusion process through the fiber mat. The absence of ink absorption for baking paper was noticed, showing the influence of the surface energy of the printing substrate during the printing process.

By printing more than one layer of ink, the metallic particles of the ink can be concentrated, leading to a continuous metallic phase after the curing process due to the sinterization of neighboring particles. Distant particles led to discontinuous electrical pathways after the curing process, affecting the final mechanical resistance and electrical conductivity of the cured pattern. This effect was clearly described by Saada et al., who noticed that the presence of cracks on the ink surface after curing affected the electrical conductivity, leading to patterns of high electrical resistance. To solve this problem, the authors proposed two strategies aiming to increase the concentration of the metallic particles and consequentially reducing the presence of cracks, increasing mechanical resistance and improving electrical properties. The authors increased the number of printed layers and the printing resolution in *DPI* (dots per inch) and tested their effect on the electrical properties. They noticed that both increasing resolution and printing multiple layers contributed to the reduction in cracks and increase in electrical conductivity [21].

Ink diffusion during the inkjet printing process using electrospun nanofiber mats as substrate was reported and studied previously. A VOC sensor with electrodes was

printed directly onto the fibers. The occurrence of ink along the width of the mat led to an increase in ink consumption during the printing process, but it also led to an increase in the conductive surface, increasing the sensitivity of the device and reducing noise [22].

In our case, the mass of the silver per printed area (m_{Ag}: [mg cm^{-2}]) can be calculated as follows:

$$m_{Ag} = \left(\frac{DPI}{2.54}\right)^2 \times N_L \times V_d \times \rho_{ink} \times X_{Ag}$$

where *DPI* is the linear printing resolution in dots per inch, 2.54 is the conversion factor to dots per cm, N_L is the number of printed layers, V_d is the drop volume in mL, ρ_{ink} is the density of the ink in g mL^{-1} and X_{Ag} is the mass fraction of silver nanoparticles in the ink. In our case, V_d can be estimated by the nominal drop volume of the nozzle (10 pL = 10^{-8} mL), and ρ_{ink} and X_{Ag} are informed by the ink vendor as 1.45 g mL^{-1} and 0.35, respectively.

By printing with a resolution of 726 *DPI*, 0.415 mg cm^{-2} of metallic silver per printed layer is deposited on the printing substrate. This leads to a maximum consumption of 2.488 mg cm^{-2} of silver in this work when six layers are printed. This consumption is close to the ink consumed by routine printing with the same ink onto a nonporous substrate such as polyethylene naphtenate (PEN) (one layer at 1693 DPI = 2.255 mg cm^{-2} of silver). A quick comparison was added in the Supplementary Materials (Table S3). Various layers of lower resolution were used in this study due to the porous nature of the PCL layer that delayed the evaporation of the ink solvent and thus led to poor print quality when optimal conditions for printing on PEN were used.

Patterns printed onto the transfer substrates with two, four and six printed layers were transferred to a 3D-printed piece and cured. Then, their electrical resistance was measured, and the results were shown in Table 1.

Table 1. Surface resistivity of transferred and cured tracks with 2, 4 and 6 printed layers using different printing substrates.

Number of printed layers	2	4	6
Donor substrate	Surface resistiviy [Ω/square]		
Kraft paper	-	-	-
Sulphite paper	-	-	-
Baking paper	43.3 ± 2.5	4.2 ± 0.5	1.9 ± 0.2

It could be observed that the surface resistivity of the patterns after curing process was dependent not only on the transfer substrate but also on the printing process (number of printed layers). Therefore, the selection of an adequate printing substrate is critical for the functionality after the curing process. The importance of the concentration of metallic nanoparticles for the formation of conductive pathways was described previously. The presence of ink absorbed in kraft paper and sulfite paper after the printing process could explain the absence of conductivity even for six printed layers. This ink could not be retained in the electrospun mats' pores and thus did not contribute to the electrical properties. On the other hand, patterns printed onto electrospun mats on baking paper as the printing substrate showed electrical conductivity with two printed layers, and the resistance was reduced twenty times by printing six layers. These results were also consistent with the absence of ink absorbed by baking paper.

Due to its effectiveness regarding the electrical properties of the printed patterns, we decided to continue using electrospun PCL on baking paper as printing substrate. Patterns with one to six printed layers were printed, transferred and cured, and the electrical conductivity was measured. The results are shown in Figure 3.

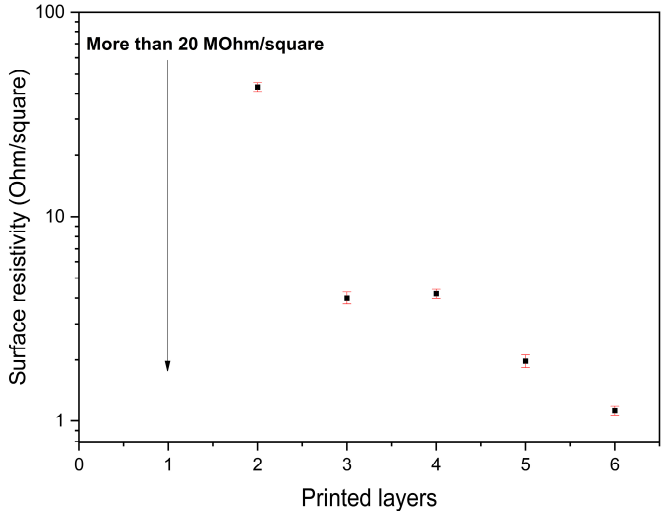

Figure 3. Surface resistivity of tracks with 1 to 6 printed layers after transfer and curing process using PCL on baking paper as printing substrate. Five samples were measured and averaged for each point.

The quantity of layers required to obtain a conductive track after the curing process depends on the local concentration of the metallic nanoparticles and also on the characteristics of the substrate [21]. For porous substrates, the ink was able to penetrate through the pores among the electrospun fibers, leading to the occurrence of different resistivity levels due to the partial filling of the pores with successive printed layers. Nonporous materials that present conductivity with only one printed layer have been reported and tested, and no diffusion effect was noticed [23,24]. In this case, three different levels of resistivity were observed at two, three and five printed layers.

A comparison of sheet resistance and trace width values obtained by various materials and techniques used in printed and conformal electronics is presented in Table 2. The trace width and resistivities achieved in this work are comparable to those in the recent literature and adequate for most applications for three and more printed layers. Moreover, resistivities were also comparable to those obtained when printing silver inks on nonporous plastic substrates such as PEN.

Table 2. Reference values of sheet resistance, trace width and postprocessing temperatures for printed and conformal electronics using different materials and techniques.

Printing Method	Printed Material	Trace Width (μm)	Sheet Resistance (Ω/square)	Postprocessing Steps	Ref.
Screen printing	Silver nanowires	30	0.64	curing at 80 °C	[25]
Copper foil (not printed)	Copper	300	n.a.	UV curing at RT	[26]
Sputtered gold (not printed)	Gold	20	5.3 [a]	(1) transfer at RT (2) evaporation of water at RT	[14]
Screen printing	Copper nanoparticles	200	0.04	Photonic sintering	[27]
Aerosol jet	Silver nanoparticles	50	0.2	Curing at 145 °C	[28] [b]
Inkjet	Silver nanoparticles	n.a.	2.8	IR curing	[29] [c]
Inkjet	Silver nanoparticles	50	1.6	curing at 145 °C	Printed tracks at our lab [d]
Inkjet	Silver nanoparticles	250	1.9	(1) transfer at 80 °C (2) curing at 145 °C	This work [e]

[a] Estimated by dividing the informed value for resistivity (5.3×10^{-7} Ω m) by the informed maximum nominal value for conductive layer thickness (100 nm). [b] The reference contains resistivity data from various commercial silver nanoparticle inks printed on silicon. The presented data corresponds to same ink and curing temperature used in this work. [c] Printed on polyethylene naphtenate, one layer, 1016 DPI. [d] Printed on polyethylene naphtenate, one layer, 1693 DPI. [e] Printed on electrospun PCL, six layers, 726 DPI.

3.2. Morphological Characterization of Transferred and Cured Tracks

Figure 4 shows the line width difference (*WD*) using different printing conditions and nominal line widths. *WD* was calculated according to the following equation:

$$WD = W\_printed - W\_design$$

where *W_printed* is the average line width calculated from 15 samples from each printed line and *W_design* is the nominal line width. The *WD* was calculated for tracks printed parallel and perpendicular to the fibers' orientation.

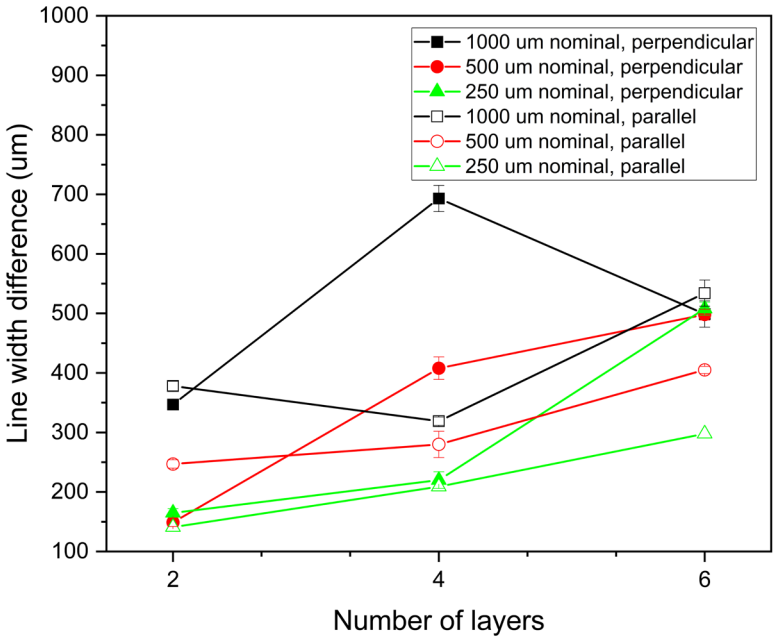

Figure 4. Line width difference as function of nominal line width, number of layers and orientation to fibers' orientation. Lines were printed onto PCL mats on baking paper.

It could be noticed that the printed lines are wider than predicted by design. This is due to the porous nature of the substrate that produces some ink spreading. The difference in line width was easily noticeable, ranging from 150 to 700 microns, and increased with nominal width and the number of printed layers, as expected. The porous characteristics of the electrospun substrate also influenced the line width difference, since it was larger when lines were printed perpendicular to the fibers. However, the line widths were reproducible, showing a maximum standard error of 22 microns. Regarding these results, it is possible to establish coherent design rules for printing conductive tracks onto electrospun PCL using silver nanoparticle inks. However, it is very important to carefully control the electrospinning process to obtain reproducible results with different batches of electrospun substrates.

Transfer and curing processes were carried out at 80 °C and 145 °C, respectively. During the transfer process, we noticed a thermal contraction effect. Dimensional differences after curing process were measure for printed patterns with 500 μm width (by design) and are shown in Table 3.

Table 3. Effect of thermal contraction of tracks after transfer and curing process depending on fiber orientation.

Number of Printed Layers	Difference ⊥ [μm]	Difference // [μm]
2	-262 ± 5	-52 ± 2
4	-95 ± 7	-27 ± 2
6	-17 ± 5	-10 ± 1

Shrinkage was observed for both senses (parallel and perpendicular to fibers' orientation) but was larger when perpendicular to the fibers, as expected, due to the pore morphology of the electrospun mat. Moreover, the shrinkage after curing was lower, as the number of printed layers increased due to the presence of higher loads of metallic nanoparticles inside the pores of the substrate.

SEM images of printed patterns with one to six printed layers before and after transfer and curing process were taken. Figure 5 compares the front and back sides of the printed PCL electrospun mat for one, three, five and six printed layers. The occurrence of an ink diffusion process by the concentration of most of ink on the back side could be observed (Figure 5E). This trend changed for three printed layers, showing both sides almost full of ink. Moreover, the saturation of the pores on the front side occurred at six printed layers (Figure 5D).

These results confirmed ink diffusion through the pores of PCL electrospun fibers. Silver ink diffusion trough porous substrates was previously reported by other authors regarding printed electronics applications [22–24]. The intensity of the diffusion process depends on the porosity and the affinity of the ink to the substrate. This phenomenon also affects the quantity of printed layers needed to obtain an electrically conductive pattern after curing.

Ink buildup allows both sides of the electrospun PCL mats to be conductive and, in turn, interconnect with each other, allowing different printed designs to be electrically connected by simply overlapping them, regardless of which is transferred first and without the need to be transferred at the same time.

Transfer and curing steps produce contraction and melting on the PCL electrospun fibers, as can be observed, especially in Figure 6A. Upon coming into contact with a piece at 80 °C, fibers melt and merge with neighboring fibers, forming larger-diameter fibers and, in turn, leaving voids on the surface. It is noteworthy that this effect decreased with increasing printed layers (Figure 6B–D). In addition, it was observed that the fibers within the ink layer did not show large structural changes after transfer at 80 °C. This phenomenon is due to the fact that the pores of the fibers are filled with silver ink, which prevents their agglomeration, maintaining a structure similar to that before the transfer.

In the case of cured fibers, thermal contraction was observed, especially in the mat with one printed layer, revealing inhomogeneities with voids of 17 μm on average. For the fibers with one layer, a rough film with holes was observed, where the fibrillar structure was completely lost. Thermal contraction was markedly lower for the fibers with three, five and six layers, where the fibrillar structure was maintained, although with the appearance of some voids. The SEM images are in accordance to the electrical resistance measurements (Figure 3) and track width measurements after curing (Table 3). Ink filling from three and more printed layers prevents the contraction of the printed tracks and provides a continuous path of sintered silver for electrical conduction.

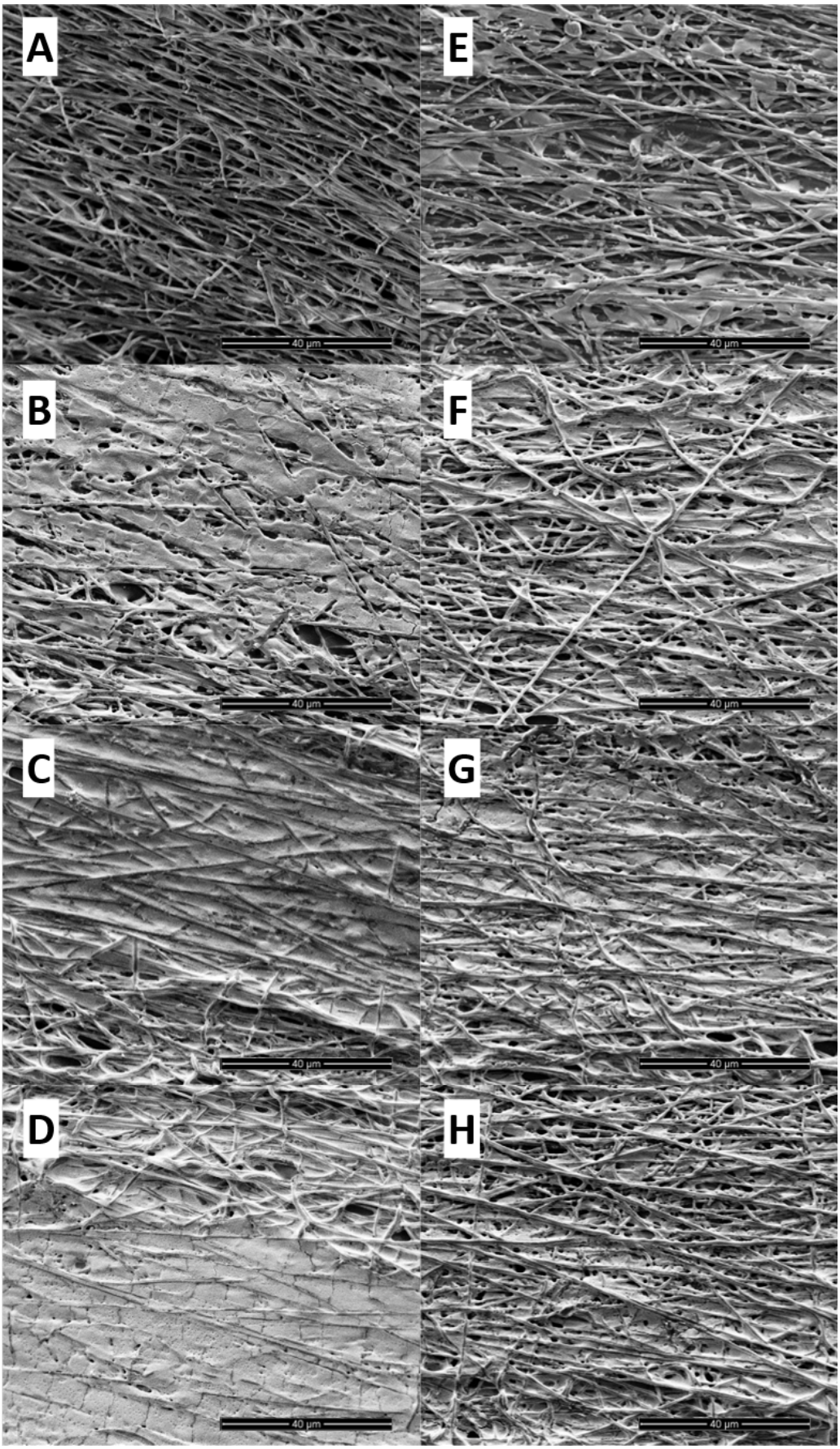

Figure 5. SEM images of both sides of a printed mat of fibers with one (**A**,**E**), three (**B**,**F**), five (**C**,**G**) and six printed layers (**E**,**H**). Front side (**A**–**D**) and back side (**E**–**H**).

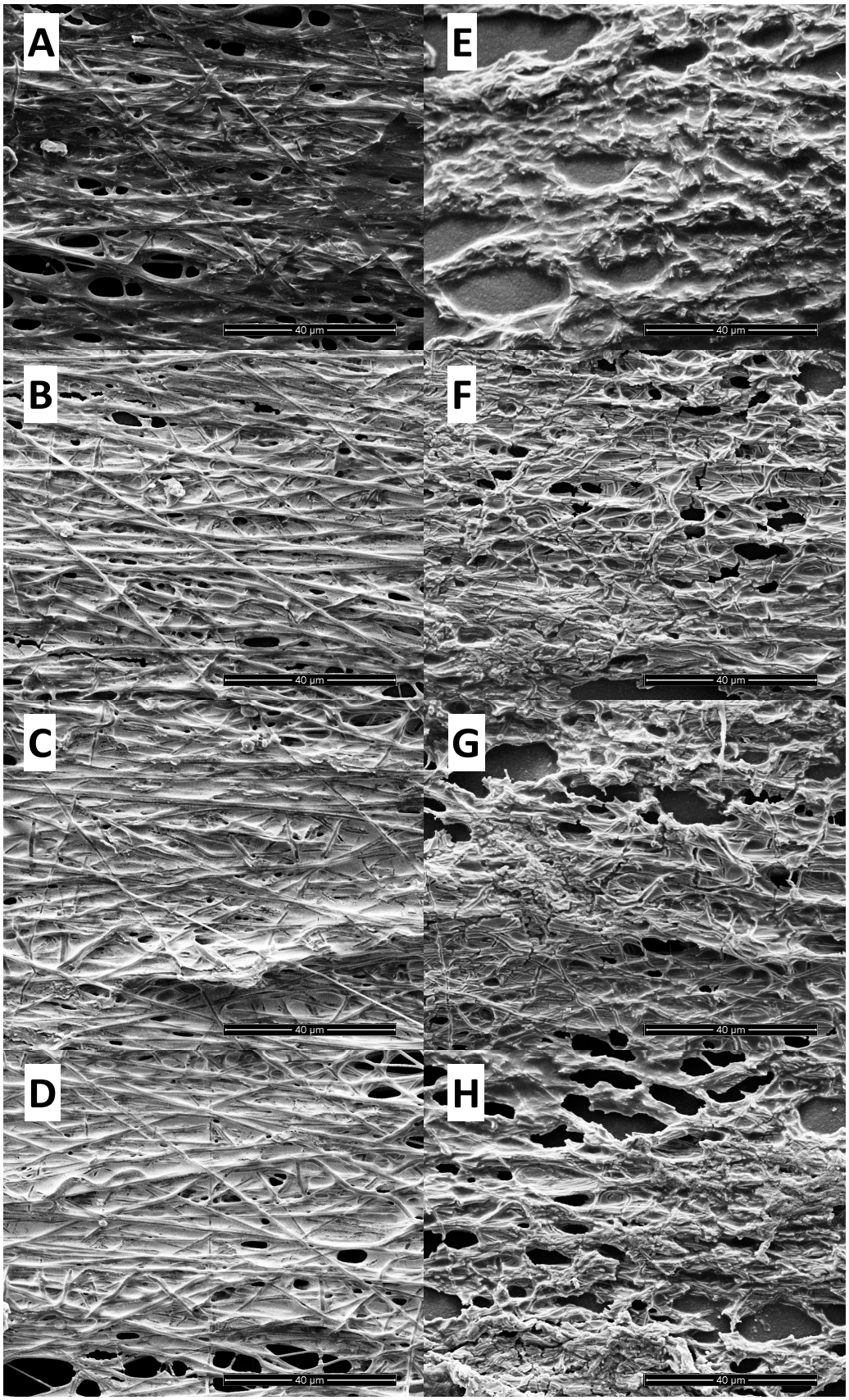

Figure 6. SEM images of the front side of a printed mat of fibers with one (**A**), three (**B**), five (**C**) and six printed layers (**D**). After transfer step (**A**–**D**) and after curing step (**E**–**H**).

The profilometry of printed tracks with two, three, four and six printed layers transferred and cured onto a PET film is shown in Figure 7.

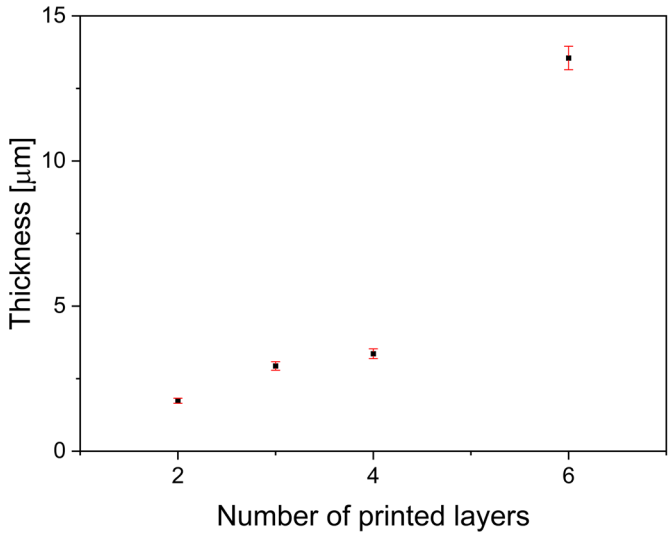

Figure 7. Thickness of printed patterns vs. printed layers after curing process. Five samples were measured and averaged for each point.

The printed tracks showed a larger thickness than the PCL electrospun mat. The two-printed-layer track was 1.74 µm thick, whereas the three- and four-layered tracks were 2.94 and 3.36 µm thick, respectively. A large increase in track thickness was observed for six printed layers (13.55 µm). This behavior could be explained by the diffusion of the ink through the porous matrix until saturation. Once the pores were fully filled with ink, each layer led to a higher thickness after the curing process.

3.3. Adherence of Printed and Transferred Patterns

To evaluate adherence and mechanical properties of the printed tracks, a rub resistance test based on standard ISO 105-A01:2010-01 [20] was performed on printed tracks with three, four and six printed layers. Printed patterns transferred to PLA 3D-printed pieces and cured were assayed using the apparatus shown in Figure 8B. The rub cycles were performed perpendicular to the track. Electrical resistant measurements were performed after 10 cycles (each cycle includes two rub steps onto the transferred design). The results of electrical resistance after rub cycles are summarized in Figure 8A.

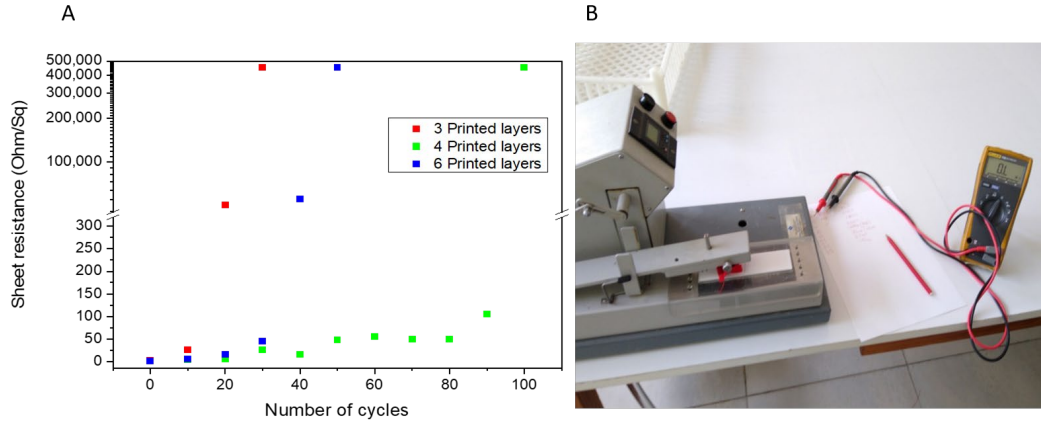

Figure 8. Sheet resistivity after incremental rub stress cycles (**A**) and rub resistance apparatus (**B**).

The samples with three layers underwent changes in their electrical resistance in the first 10 cycles, increasing the resistance by one order of magnitude, while, after 20 cycles,

the increase in electrical resistance was three orders of magnitude, losing all functionality after 30 cycles. The samples with four and six layers showed practically no change until after 20 cycles. After 30 cycles, an order-of-magnitude increase in resistance was observed in both samples. Samples with four layers remained close to that value until after 80 cycles and lost functionality after 100, while the samples with six layers began to lose functionality after 40 cycles with an increase in electrical resistance of four orders of magnitude and lost it completely after 50 cycles.

The rub resistance test shows that increasing the number of layers has consequences on mechanical properties and cohesion, as well as electrical conductivity. To understand this behavior regarding rubbing and the failure mechanism, SEM images of all the samples that were subjected to rubbing were taken, and the images before and after failure were compared. Figure 9A shows images of the zone subjected to rubbing before and after the loss of functionality due to rubbing the lines with three, four and six layers.

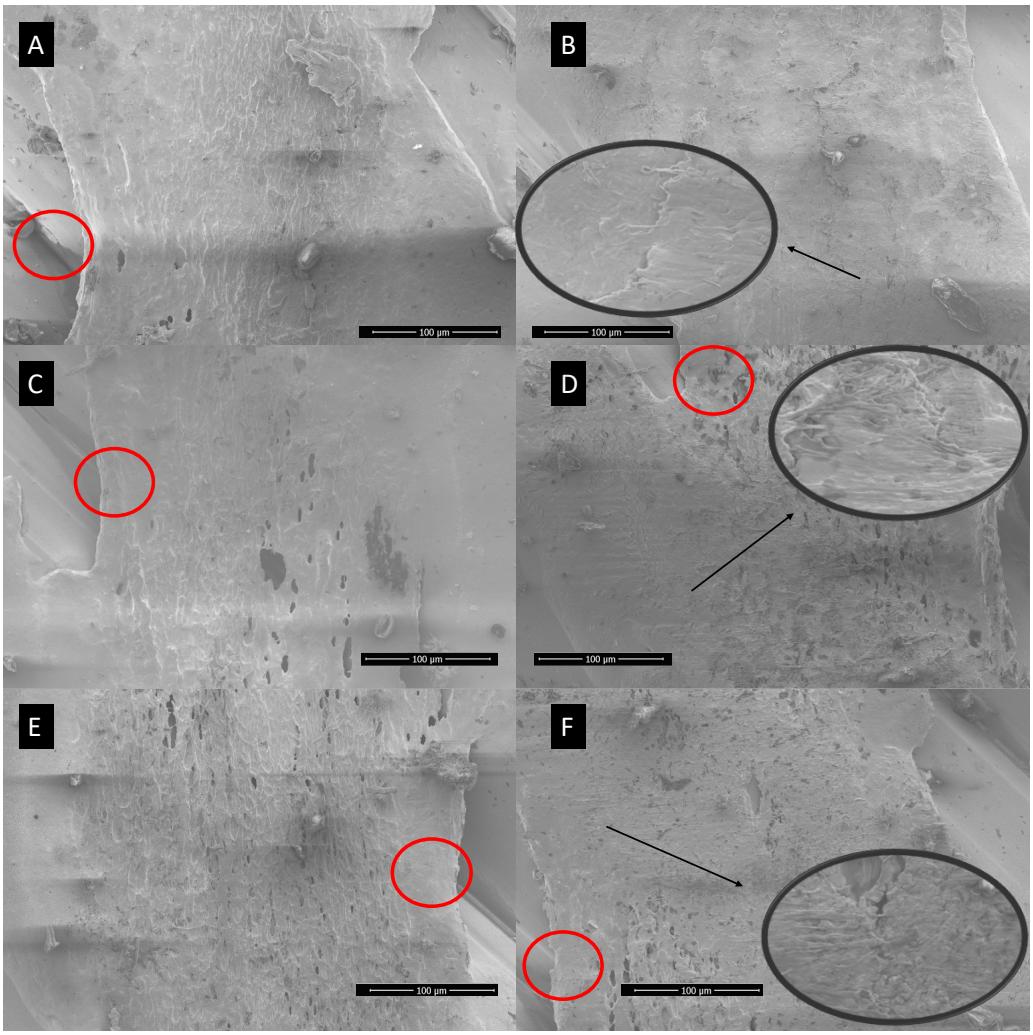

Figure 9. SEM before and after the loss of functionality due to rubbing for the lines with three (**A**,**B**), four (**C**,**D**) and six layers (**E**,**F**). Red circles show grooves on the FDM printed surface and black circles with pointing arrows show dragging of the electrospun material at the ridges.

SEM images after rubbing (Figure 9) show that tracks were affected by rubbing. The printed silver layer has been dragged with the passes in every case. It was also observed that there is an influence of the 3D-printed layer on the rub resistance. This is because fused-filament 3D printing is an additive technique that fuses filament lines one beside the other, inevitably leaving grooves and ridges along the surface. It is clearly observed that

the fibers attached to a groove sector remained adhered to the 3D-printed surface, while those on a ridge were pulled out from the surface.

The results can be explained through considering that the ink layers are sintered. By increasing the thickness of the layer, there is a higher concentration of particles and, therefore, better initial conductivity. On the other hand, a thicker layer of sintered ink has greater resistance to rubbing. It is expected that the ink layer will remain cohesive against the shear stress that occurs during rubbing. First, the greater the number of layers, the larger the thickness of the cured pattern. Therefore, the resistance increases more with higher number of layers, due to higher shear stress, as exemplified in Figure 10. On the other hand, by increasing the number of printed layers, saturation of the pores with ink was observed. The greater the saturation of the pores, the greater the mechanical resistance to shearing of the pattern, because it will have less chance of deformation as the cloth passes.

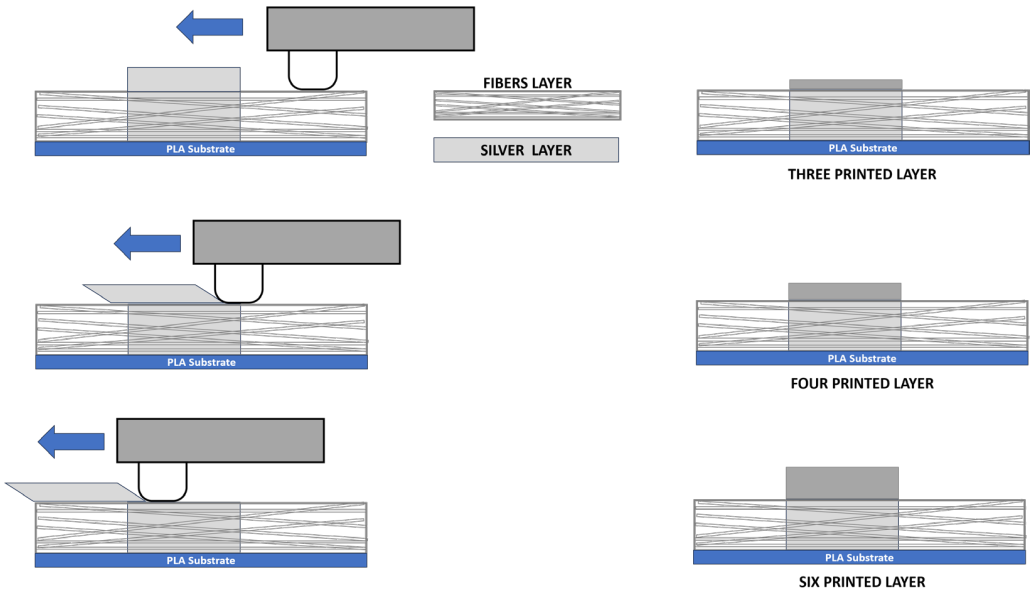

Figure 10. Schema of the proposed mechanism of failure by rubbing.

The first mechanism allows us to explain the differences between the samples with three and four layers and the one with six layers, where a difference of 300% was observed in the thickness of the conductive silver track. On the other hand, the thickness of the deposit with three and four layers presented little variation among themselves. The tracks with six layers, although presenting a more solid structure due to having a greater filling of the pores, has a much greater thickness that generates a larger shear stress during rubbing. Although there were no significant differences in thickness between the tracks with three and four layers, the track printed with four layers will have a higher saturation of silver particles within the fibers, and thus the accumulation of particles not only generates more conductive channels but also gives greater toughness to the mechanical assembly formed by the fibers and the neighboring sintered silver nanoparticles. This feature allowed the system with four layers to achieve greater resistance to rubbing cycles.

Adherence tests were performed on traces printed with different numbers of layers and transferred to PLA pieces. Scotch tape was used to peel off weakly bound material from the surface. The results are presented in Figure 11.

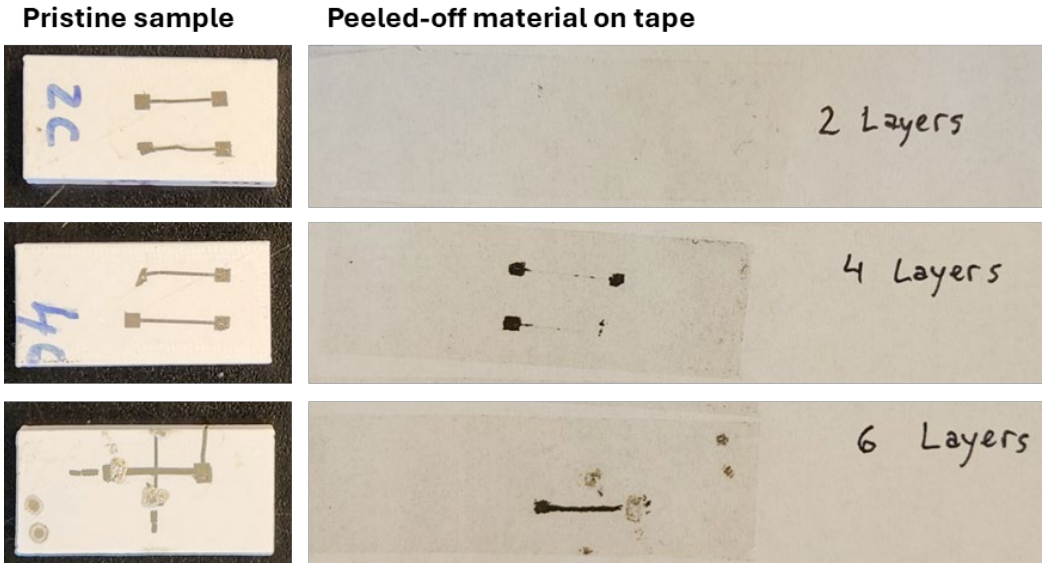

Figure 11. PLA pieces with transferred and cured conductive printed traces with two, four and six layers (**left**) and the corresponding tapes with removed material after adhesion tests (**right**).

It could be noticed that for two layers the tape did not remove a significant amount of material. The traces remained conductive after the test, although they maintained a relatively high resistivity of 40 Ω/square. On the other hand, traces printed with four and six layers were subjected to intensive remotion of printed silver, leading to a loss of conductivity. These results are coherent with the hypothesis of the ink filling and saturating the pores of the PCL mat derived from resistivity measurements, profilometry, SEM images and the rub resistance test. Traces with two printed layers retain most of the ink within the PCL pores, which results in relatively high sheet resistance but strong adherence of the silver to PCL and PLA. On the other hand, traces printed with four and six layers show sheet resistance comparable to that of traces printed on nonporous substrates, because PCL pores are completely saturated with ink and thus a continuous layer of silver can be formed on top of the PCL layer. However, these conductive layers are not as mechanically stable as those printed with two layers.

3.4. Tracks Transferred to Non-Planar Surfaces and Flexible Acceptor Substrates

In order to demonstrate the application of the transfer to different topologies and receptor substrates, different printed patterns were printed and transferred to PLA 3D-printed surfaces (planar, with concavities and sharp edges), flexible PET film and elastic TPU film, as shown in Figure 12.

All the patterns showed electrical conductivity after the curing process, regardless of the topology and composition of the receptor substrate. The electrical conductivity of the tracks transferred to flexible substrates of PET and TPU was measured with mean values of 3 and 4 Ω/Square, respectively, and they maintained their conductivity after bending.

The occurrence of the ink diffusion process led to the presence of ink on both sides of the fiber mat, which allows the connection of two different printed tracks that are transferred separately. In order to prove this assumption, different printed patterns were transferred, partially overlapping one on top of the other, and cured in separate steps, as shown in Figure 12D. Their electrical surface resistivities are summarized in Table 4.

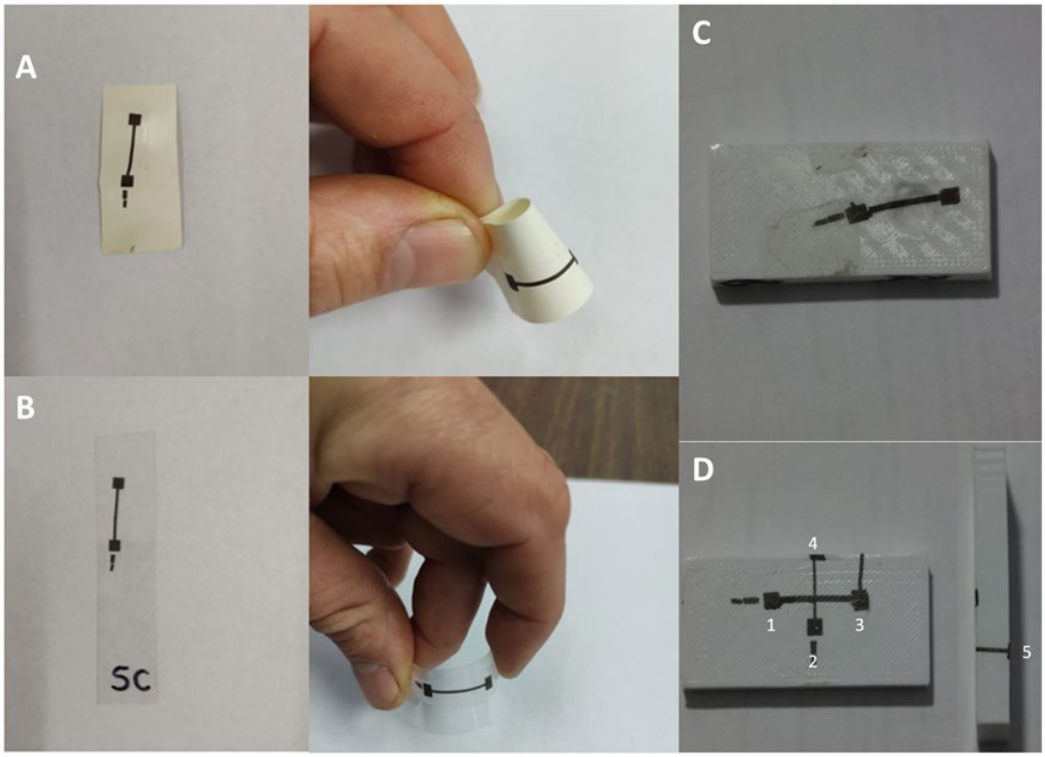

Figure 12. Tracks with six printed layers transferred to flexible TPU substrate (**A**), PET substrate (**B**), non-planar 3D-printed PLA substrate (**C**) and 90°-angle 3D-printed PLA substrate (**D**).

Table 4. Summarized electrical properties of tracks transferred and cured separately for newly fabricated devices and the same after two years (see Figure 12D for reference). Five measurements were averaged for each point.

Track	Sheet Resistance [Ω/square] (Newly Fabricated)	Sheet Resistance [Ω/square] (After Two Years)
2-4	2.0 ± 0.3	1.9 ± 0.3
1-3	0.9 ± 0.1	1.2 ± 0.2
2-1	1.7 ± 0.2	1.7 ± 0.2
4-1	1.9 ± 0.3	1.9 ± 0.2
2-3	2.0 ± 0.1	2.0 ± 0.2
4-3	1.7 ± 0.2	1.8 ± 0.2
3-5	1.1 ± 0.2	1.1 ± 0.2
1-5	3.1 ± 0.3	3.3 ± 0.3
2-5	5.7 ± 0.7	6.0 ± 0.6

Electrical continuity was verified even after connecting patterns in different transfer and curing steps or by transferring a printed track from one side to the opposite of the 3D-printed piece, passing by sharp 90-degree edges. Thus, this system demonstrated to be modular and adaptable to different surface topologies. Modularity is a desirable property in this kind of system due to the possibility of modifying, enlarging or repairing previously transferred and cured circuits.

An interesting feature arises from the adhesion test performed on the modular system (Figure 11, six layers). The removal of material occurred only in the trace that was placed on top, which indicates that the transfer of a PCL electrospun mat on top of a conductive trace serves as a protective layer that enhances the mechanical stability of the conductive material. These conductive traces were demonstrated to be stable over time. The resistivity of the same conductive printed tracks was measured after two years and did not show any significant differences.

3.5. Transference of an Interdigitated Electrode onto Nonplanar 3D-Printed PLA Substrates

In order to determine the performance of the printing and transfer process, an interdigitated electrode with W/L = 220 was printed and transferred to a 3D-printed surface with a concavity. Concavities printed using 3D printing process could lead to the occurrence of a rough surface. Problems with rough surfaces were also reported by other authors and solved by polishing the surface or by adding a levelling layer with another material before the transfer process [21]. The surface of the concavity was polished to minimize the presence of printed-layer imperfections, minimizing the occurrence of defects on the fingers of the interdigitated electrode. The printing, transfer and curing process is shown in Figure 13.

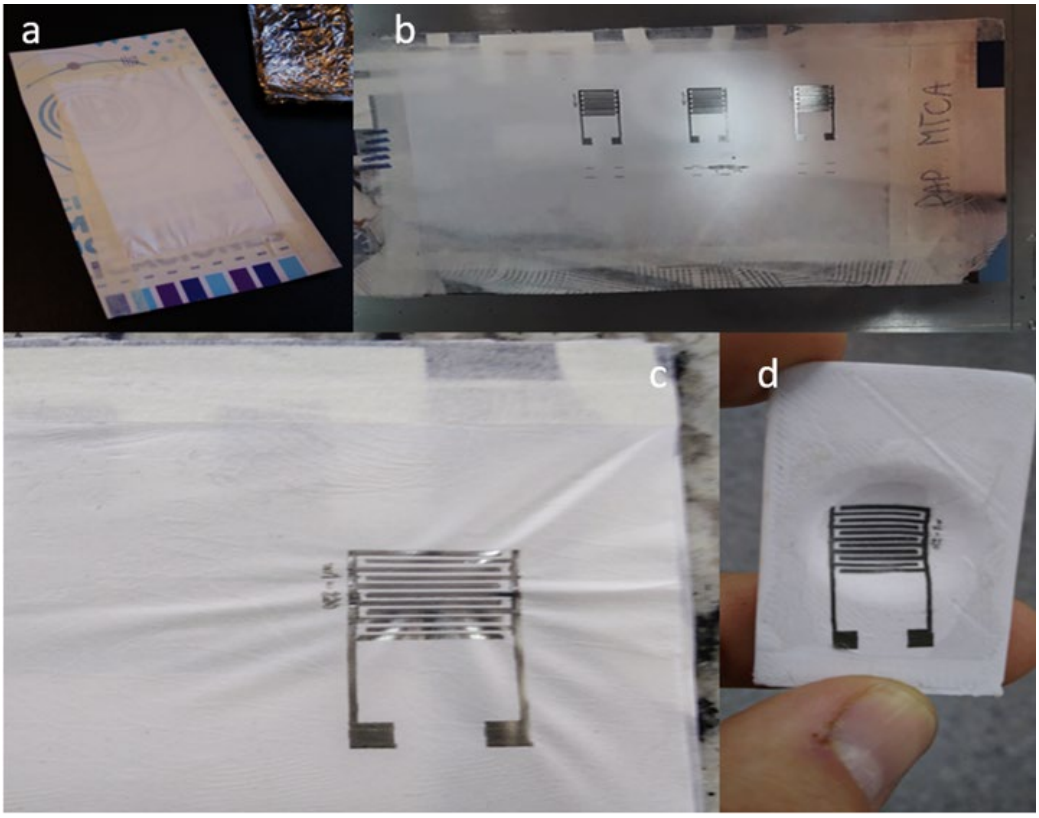

Figure 13. Printing transfer and curing process of an interdigitated electrode onto a 3D-printed PLA substrate with a cavity. (**a**) As-spun fibers on baking paper and prepared for the printing process. (**b**,**c**) Electrodes printed onto the PCL fibers. (**d**) Three-dimensionally printed piece with an interdigitated electrode on a concave surface after the transfer and curing process.

The transferred interdigitated electrode was tested as a capacitive touch sensor to sense the presence of a finger in the cavity. The sensor showed an increment of 22 pF when a finger was pressed onto the sensor. Therefore, this transfer system is potentially attractive as an economic way of incorporating capacitive sensors or circuits into previously molded non-flat pieces (industry for the fabrication of touch buttons or LED lighting circuits).

4. Conclusions

A novel thermal transfer method of electrically conductive metallic silver patterns printed with inkjet printing onto mats of PCL fibers fabricated by electrospinning using nonplanar pieces as a receptor substrate was developed. The printing substrate and the printing conditions were optimized in order to obtain an electrically conductive and reproducible printed pattern. It was found that baking paper could be used underneath the electrospun PCL mat in order to retain silver nanoparticle ink within the pores of the

electrospun mat, and at least two layers had to be printed in order to provide electrical conductivity. Moreover, when four or more layers were printed, the sheet resistivity of the printed traces was close to that obtained by printing onto nonporous plastic substrates. It was shown that the number of printed layers affected not only the final functionality but also the final mechanical stability of the design. On the other hand, the presence of a diffusive process of the ink through the pores of the fiber mat was observed. This ink diffusion led to tracks that were wider than predicted by design but reproducible. This process also rendered both sides of the PCL electrospun mat conductive, which in turn allowed the electrical connection of different printed patterns that were transferred separately. Moreover, the printed tracks could be transferred to nonplanar surfaces along sharp edges, retaining electrical connection. These features allow the use of this transfer system for the creation of modular interconnection in complex nonplanar pieces.

The rub resistance of tracks cured with different numbers of printed layers was also evaluated, and it was found that the system was able to withstand the rubbing of a microfiber cloth and retain electrical continuity even after 160 passes. Adhesion resistance proved to be dependent on the number of printed layers: two printed layers led to less conductive traces, although they were mechanically stable, whereas four or more printed layers led to higher conductivity and lower adhesion resistance. The transferred traces also demonstrated to be stable over time, maintaining the same sheet resistance even two years after being printed. Such a transfer system is presented as a potential alternative for application in topologies where conventional techniques such as inkjet printing or stamping show difficulties, for example, in fabrication of electronics as capacitive touch panels on molded parts with application in the automotive industry, among others.

Supplementary Materials: The following supporting information can be downloaded at: https://www.mdpi.com/article/10.3390/applnano6020010/s1, Figure S1: SEM images of the printed face of the fibers with one (a), two (b), three (c), four (d), five (e) and six printed layers (f); Figure S2: SEM images of the opposite face of printed fibers with one (a), two (b), three (c), four (d), five (e) and six printed layers (f); Figure S3: SEM images of transferred fibers with one (a), two (b), three (c), four (d), five (e) and six printed layers (f); Figure S4: SEM images of cured fibers with one (a), two (b), three (c), four (d), five (e) and six printed layers (f); Figure S5: SEM images of the cured fibers with three, four and six printed layers before (a,d,g) and after the rub resistance test in the groove (b,e,h) and ridge (c,f,i) zone; Figure S6: SEM images of the printed face of fibers with six printed layers with 3000× (a), 24,000× (b) and 100,000× (c). Figures S6b,c evidence the presence of the nanoparticles of silver; Table S1: Summary of mean values and SD of the electrical resistance measurements reported in Figure 3; Table S2: Summary of mean values and SD of the thickness reported in Figure 7; Table S3: Mass of silver per printed area and resistivity for inkjet-printed silver ink in different conditions.

Author Contributions: Conceptualization, F.N.M. and L.N.M.; methodology, F.N.M. and E.B.; validation, F.N.M. and E.B.; formal analysis, F.N.M. and L.N.M.; investigation, F.N.M., E.B. and L.N.M.; resources, L.N.M.; data curation, F.N.M., E.B. and L.N.M.; writing—original draft preparation, F.N.M., E.B. and L.N.M.; writing—review and editing, F.N.M., E.B. and L.N.M.; visualization, F.N.M. and L.N.M.; supervision, L.N.M.; project administration, L.N.M.; funding acquisition, L.N.M. All authors have read and agreed to the published version of the manuscript.

Funding: This research was funded by INTI, ANPCyT (PICT 2013-0427, PICT 2014-3748 and PICT 2017-2787) and CONICET (PIP 11220150100967).

Data Availability Statement: Data is contained within the article or Supplementary Materials. The data presented in this study are available in article or Supplementary Materials.

Acknowledgments: We thank INTI, ANPCyT (PICT 2013-0427, PICT 2014-3748 and PICT 2017-2787) and CONICET (PIP 11220150100967) for financial support. LNM is part of the research staff

of CONICET. Authors are grateful to Theo Rodríguez Campos for the measurements of printed line widths.

Conflicts of Interest: The authors declare no conflicts of interest.

References

1. Jian, J.R.; Kim, T.; Park, J.S.; Wang, J.; Kim, W.S. High performance 3D printed electronics using electroless plated copper. *AIP Adv.* **2017**, *7*, 035314. [CrossRef]
2. Keranen, A.; Heikkinen, M.; Raappana, P.; Saaski, J. Method and Arrangement for Providing Electrical Connection to In-Mold-Electronics. U.S. Patent 2017/0215756A1, 3 August 2017.
3. Jo, Y.; Kim, J.Y.; Jung, S.; Ahn, B.Y.; Lewis, J.A.; Choi, Y.; Jeong, S. 3D polymer objects with electronic components interconnected: Via conformally printed electrodes. *Nanoscale* **2017**, *9*, 14798–14803. [CrossRef] [PubMed]
4. Chen, I.M.; Liu, Y.; Yu, X.; Everhart, W.; Park, J.; Wang, Y.; Pan, H. Aerosol printing and flash sintering of conformal conductors on 3D nonplanar surfaces. *Manuf. Lett.* **2022**, *31*, 119–123. [CrossRef]
5. Lewis, J.A.; Ahn, B.Y. Three-dimensional printed electronics. *Nature* **2015**, *518*, 42–43. [CrossRef] [PubMed]
6. Park, J.S.; Kim, T.; Kim, W.S. Conductive Cellulose Composites with Low Percolation Threshold for 3D Printed Electronics. *Sci. Rep.* **2017**, *7*, 3246. [CrossRef]
7. Sowade, E.; Polomoshnov, M.; Willert, A.; Baumann, R.R. Toward 3D-Printed Electronics: Inkjet-Printed Vertical Metal Wire Interconnects and Screen-Printed Batteries. *Adv. Eng. Mater.* **2019**, *21*, 1900568. [CrossRef]
8. Flowers, P.F.; Reyes, C.; Ye, S.; Kim, M.J.; Wiley, B.J. 3D printing electronic components and circuits with conductive thermoplastic filament. *Addit. Manuf.* **2017**, *18*, 156–163. [CrossRef]
9. Yu, X.; Liu, Y.; Pham, H.; Sarkar, S.; Ludwig, B.; Chen, I.; Everhart, W.; Park, J.; Wang, Y.; Pan, H. Customizable Nonplanar Printing of Lithium-Ion Batteries. *Adv. Mater. Technol.* **2019**, *4*, 1900645. [CrossRef]
10. Izumi, K.; Yoshida, Y.; Tokito, S. Soft blanket gravure printing technology for finely patterned conductive layers on three-dimensional or curved surfaces. *Jpn. J. Appl. Phys.* **2017**, *56*, 05EA03. [CrossRef]
11. Bakr, M.; Su, Y.; Bossuyt, F.; Vanfleteren, J. Effect of overmolding process on the integrity of electronic circuits. In Proceedings of the 2019 22nd European Microelectronics and Packaging Conference & Exhibition (EMPC), Pisa, Italy, 16–19 September 2019. [CrossRef]
12. Sundaram, S.; Kim, D.S.; Baldo, M.A.; Hayward, R.C.; Matusik, W. 3D-Printed Self-Folding Electronics. *ACS Appl. Mater. Interfaces* **2017**, *9*, 32290–32298. [CrossRef]
13. Wang, C.; Sim, K.; Chen, J.; Kim, H.; Rao, Z.; Li, Y.; Chen, W.; Song, J.; Verduzco, R.; Yu, C. Soft Ultrathin Electronics Innervated Adaptive Fully Soft Robots. *Adv. Mater.* **2018**, *30*, 1706695. [CrossRef] [PubMed]
14. Miyamoto, A.; Lee, S.; Cooray, N.F.; Lee, S.; Mori, M.; Matsuhisa, N.; Jin, H.; Yoda, L.; Yokota, T.; Itoh, A.; et al. Inflammation-free, gas-permeable, lightweight, stretchable on-skin electronics with nanomeshes. *Nat. Nanotechnol.* **2017**, *12*, 907–913. [CrossRef]
15. Molinari, F.N.; Barragán, E.; Bilbao, E.; Patrone, L.; Giménez, G.; Medrano, A.V.; Tolley, A.; Monsalve, L.N. *An Electrospun Polymer Composite with Fullerene-Multiwalled Carbon Nanotube Exohedral Complexes Can Act as Memory Device*; Elsevier Ltd.: Amsterdam, The Netherlands, 2020. [CrossRef]
16. Molinari, F.; Medrano, A.V.; Bacigalupe, A.; Escobar, M.; Monsalve, L.N. Different dispersion states of MWCNT in aligned conductive electrospun PCL/MWCNT composites. *Fuller. Nanotub. Carbon Nanostruct.* **2018**, *26*, 667–674. [CrossRef]
17. Pastore Carbone, M.G.; Di Maio, E.; Scherillo, G.; Mensitieri, G.; Iannace, S. Solubility, mutual diffusivity, specific volume and interfacial tension of molten PCL/CO_2 solutions by a fully experimental procedure: Effect of pressure and temperature. *J. Supercrit. Fluids* **2012**, *67*, 131–138. [CrossRef]
18. Lin, W.; Shen, H.; Xu, G.; Zhang, L.; Fu, J.; Deng, X. Single-layer temperature-adjusting transition method to improve the bond strength of 3D-printed PCL/PLA parts. *Compos. Part A Appl. Sci. Manuf.* **2018**, *115*, 22–30. [CrossRef]
19. Saniei, H.; Mousavi, S. Surface modification of PLA 3D-printed implants by electrospinning with enhanced bioactivity and cell affinity. *Polymer* **2020**, *196*, 122467. [CrossRef]
20. *ISO 105-A01:2010-01*; Textiles—Tests for colour fastness—Part A01: General principles of testing (6th ed.). International Organization for Standardization: Geneva, Switzerland, 2010.
21. Saada, G.; Layani, M.; Chernevousky, A.; Magdassi, S. Hydroprinting Conductive Patterns onto 3D Structures. *Adv. Mater. Technol.* **2017**, *2*, 1600289. [CrossRef]
22. Han, L.; Andrady, A.; Guzan, K.; Ensor, D. Electrospun composite nanofibers for sensor applications. *MRS Online Proc. Libr.* **2009**, *927*, 1240. [CrossRef]
23. Zhu, D.; Wu, M. Highly Conductive Nano-Silver Circuits by Inkjet Printing. *J. Electron. Mater.* **2018**, *47*, 5133–5147. [CrossRef]
24. Joubert, T.H.; Bezuidenhout, P.H.; Chen, H.; Smith, S.; Land, K.J. Inkjet-printed Silver Tracks on Different Paper Substrates. *Mater. Today Proc.* **2015**, *2*, 3891–3900. [CrossRef]

25. Mi, X.; Liu, L.; Yang, S.; Wu, P.; Zhan, W.; Ji, X.; Liang, J. Ink formulation of functional nanowires with hyperbranched stabilizers for versatile printing of flexible electronics. *Nat. Commun.* **2025**, *16*, 2590. [CrossRef] [PubMed]
26. Chen, X.; Jian, W.; Wang, Z.; Ai, J.; Kang, Y.; Sun, P.; Wang, Z.; Ma, Y.; Wang, H.; Chen, Y.; et al. Wrap-like transfer printing for three-dimensional curvy electronics. *Sci. Adv.* **2023**, *9*, eadi0357. [CrossRef] [PubMed]
27. Abbas, B.; Jewell, E.; Lau, Y.C.; Searle, J.; Claypole, T. Photonic sintering of copper for rapid processing of thick film conducting circuits on FTO coated glass. *Sci. Rep.* **2023**, *13*, 5080. [CrossRef] [PubMed]
28. Deneault, J.R.; Bartsch, C.; Cook, A.; Grabowski, C.; Berrigan, J.D.; Glavin, N.; Buskohl, P.R. Conductivity and radio frequency performance data for silver nanoparticle inks deposited via aerosol jet deposition and processed under varying conditions. *Data Br.* **2020**, *33*, 106331. [CrossRef]
29. Mitra, K.Y.; Weise, D.; Hartwig, M.; Kapadia, S.; Baumann, R.R. Time-Efficient Curing of Printed Dielectrics via Infra-Red Suitable to S2S and R2R Manufacturing Platforms for Electronic Devices. *IEEE Trans. Electron Devices* **2016**, *63*, 2777–2784. [CrossRef]